SUPPORTING INFORMATION FOR

Substrate-triggered Formation of a Peroxo-Fe_2(III/III) Intermediate during Fatty Acid Decarboxylation by UndA

Bo Zhang,[1,#] Lauren J. Rajakovich,[2,†,#] Devon van Cura,[1,†] Elizabeth J. Blaesi,[1,⊥] Andrew J. Mitchell,[2,‖] Christina R. Tysoe,[1] Xuejun Zhu,[3] Bennett R. Streit,[1,§] Zhe Rui,[3] Wenjun Zhang,[3,*] Amie K. Boal,[1,2,*] Carsten Krebs,[1,2,*] and J. Martin Bollinger, Jr.[1,2,*]

[1]Department of Chemistry and [2]Department of Biochemistry and Molecular Biology, The Pennsylvania State University, University Park, Pennsylvania 16802

[3]Department of Chemical and Biomolecular Engineering, University of California, Berkeley, California 94720

[†]Present address: Department of Chemistry and Chemical Biology, Harvard University, Cambridge, Massachusetts 02138

[⊥]Present address: GlaxoSmithKline, 1250 S. Collegeville Rd, Collegeville, Pennsylvania 19426

[‖]Present address: Whitehead Institute for Biomedical Research, Cambridge, Massachusetts 02142

[§]Present address: Department of Chemistry and Biochemistry, Montana State University, Bozeman, Montana 59717

[#]These authors contributed equally.

***Corresponding Authors**
wjzhang@berkeley.edu
akb20@psu.edu
jmb21@psu.edu
cdk10@psu.edu

Table of Contents

EXPERIMENTAL SECTION

Materials. Technical grade (> 85% purity) sodium hydrosulfite (dithionite), lauric acid, and tergitol NP-40 were purchased from Sigma-Aldrich (St. Louis, USA). All other chemicals used for protein over-expression and purification were purchased from Sigma-Aldrich (St. Louis, USA), unless stated otherwise.

DNA Constructs for over-expression of His_6-tagged UndA and variants. Construction of the plasmid containing the gene encoding full-length *Pseudomonas fluorescens* Pf-5 UndA with N-terminal His_6-tag was described previously.[1] The change in the codon for W190 to encode Phe was generated using the Thermo Scientific Phusion Site-Directed Mutagensis kit and primers listed in Table S1. The phenylalanine substitutions of Y71, Y107, and Y197 and the alanine substitutions of Glu159, His201, and Asp198 were generated by using the QuikChange site-directed mutagenesis kit and the primers listed in Table S1. Plasmid sequences were confirmed by the Penn State University Nucleic Acid Facility.

Over-expression and purification of His_6-tagged UndA and variants. The plasmids encoding wild-type UndA or its variants were used to transform *Escherichia coli* (*Ec*) BL21 (DE3) competent cells (Invitrogen; Carlsbad, CA). Transformed cells with kanamycin resistance were cultured at 37 °C with shaking (250 rpm) in either rich Luria Broth (LB) medium with 50 mg/L kanamycin or minimal (M9) medium with 0.2% (v/v) glucose, 0.10 mM $CaCl_2$, 200 mM $MgSO_4 \cdot 7H_2O$, 0.125 mM $(NH_4)_2Fe(SO_4)_2 \cdot 6H_2O$, and 50 mg/L kanamycin. At an OD_{600} of 0.6-0.8, protein expression was induced by addition of IPTG to a concentration of 0.25 mM. M9 medium cultures were supplemented with an additional 0.125 mM $(NH_4)_2Fe(SO_4)_2 \cdot 6H_2O$ at this time. The cultures were then incubated at 18 °C with shaking (250 rpm) for 18 h and harvested by centrifugation at 8,000*g* for 15 min at 4 °C. Cell pellets were flash frozen in liquid N_2 and stored at -80 °C until further use. UndA protein enriched with ^{57}Fe was expressed in M9 medium supplemented with 0.050 mM $^{57}FeSO_4$ [prepared by dissolving ^{57}Fe metal (ISOFLEX USA) in 2 M H_2SO_4] at the time of inoculation and again at the time of induction. In this case, $(NH_4)_2Fe(SO_4)_2 \cdot 6H_2O$ was not included in the culture medium.

Cells were re-suspended in lysis buffer [100 mM *tris*-(hydroxymethyl)aminomethane (Tris)-

HCl (pH 8.5) buffer, 300 mM NaCl, and 10% glycerol] at a ratio of approximately 10 mL buffer per 1 g of wet cell mass. The suspension was lysed by passage through a Microfluidics M-110EH-30 microfluidizer processor at 20,000 psi for 10 min and centrifuged at 22,000*g* for 20 min at 4 °C. The supernatant was loaded onto a Ni^{2+}-NTA immobilized affinity chromatography column (~20 mL resin per 100 mL lysate) pre-equilibrated with lysis buffer. After loading, 5 column volumes of wash buffer [100 mM Tris-HCl (pH 8.5), 300 mM NaCl, 50 mM imidazole and 10% glycerol] was passed through the column to remove unspecifically bound protein. Elution was achieved by passing elution buffer [100 mM Tris-HCl (pH 8.5) buffer, 300 mM NaCl, 250 mM imidazole, and 10% glycerol] over the column. Fractions containing the protein of interest were combined and concentrated at 3,500*g* using a 10K MWCO Macrosep® Advance Centrifugal Device (Pall Corporation, Port Washington, New York). The concentrated protein was then dialyzed three times (4 h each) against 100 equivalent volumes of lysis buffer. Protein for crystallography was further purified by size exclusion chromatography using a Sephadex S-200 column (120 mL resin) equilibrated with lysis buffer. The protein was frozen in liquid N_2 and stored at -80 °C.

Protein purity was assessed by SDS-PAGE with Coomassie staining, and protein concentration was determined by using a molar absorption coefficient of 70,980 $M^{-1}cm^{-1}$ at 280 nm. The iron content in the purified protein was quantified either by inductively coupled plasma – atomic emission spectroscopy (ICP-AES) at the Penn State Materials Research Institute or colorimetrically by the ferrozine assay.[2] Protein over-expressed in LB medium typically contained < 0.04 Fe/protein and was considered to be "apo". Protein over-expressed in Fe-supplemented M9 minimal medium typically had 0.5-1.0 Fe/protein. Following the aerobic purification, subsequent handling of UndA protein samples, including reduction and reconstitution described below, were carried out inside an anoxic chamber (Labmaster, MBraun, Stratham, USA).

^{57}Fe Mössbauer Spectroscopy. Mössbauer spectra were recorded on spectrometers from SEECO (Edina, MN). The spectrometer used to acquire the weak-field spectra is equipped with a Janis SVT-400 variable-temperature cryostat. The spectrometer used to acquire the weak-field spectra is equipped with a Janis 8TMOSS-OM-12SVT variable-temperature cryostat. The external magnetic field was applied parallel to the γ beam. All isomer shifts quoted are relative to the centroid of the spectrum of α-iron metal at room temperature. Simulations of Mössbauer spectra

were carried out with the WMOSS spectral analysis software (www.wmoss.org, WEB Research, Edina, MN).

Simulations of spectra obtained in strong applied magnetic field are based on the commonly used spin Hamiltonian (Eq. 1), in which the first three terms quantify the electron Zeeman effect and zero field splitting (ZFS) of the electron-spin ground state, the fourth term represents the interaction between the electric field gradient and the nuclear quadrupole moment, the fifth term describes the magnetic hyperfine interactions of the electronic spin with the ^{57}Fe nucleus, and the last term represents the ^{57}Fe nuclear Zeeman interaction.

$$\begin{aligned}\mathbf{H} = \beta \mathbf{S} \bullet \mathbf{g} \bullet \mathbf{B} + D\left(\mathbf{S}_z^2 - \frac{S(S+1)}{3}\right) + E\left(\mathbf{S}_x^2 - \mathbf{S}_y^2\right) \\ + \frac{\mathbf{eQV}_{zz}}{4}\left[\mathbf{I}_z^2 - \frac{I(I+1)}{3} + \frac{\eta}{3}\left(\mathbf{I}_x^2 - \mathbf{I}_y^2\right)\right] + \mathbf{S} \bullet \mathbf{A} \bullet \mathbf{I} - g_n \beta_n \mathbf{B} \bullet \mathbf{I}\end{aligned} \qquad \text{(Eq. 1)}$$

Continuous-wave (CW) EPR Spectroscopy. X-Band (~ 9.5 GHz) EPR spectra were acquired on a Bruker ESP-300 spectrometer equipped with an ER/4102 ST resonator (Bruker), an Oxford Instruments continuous helium flow cryostat, and an Oxford Instruments temperature controller (ITC 502). Quartz tubes (QSI) with 3 mm inner and 4 mm outer diameter were used for all experiments. Quantification of EPR signals was achieved by double integration of first-derivative EPR spectra and comparison to signals from a Cu^{2+} standard with concentration of 256.0 uM (for wild-type UndA experiments) or 102.5 uM (for W190F UndA experiments), measured under non-saturating conditions. A packing factor of 0.5 was used for spin quantification of EPR spectra of freeze-quenched samples.

X-ray absorption spectroscopy (XAS). Samples of aerobically isolated or dithionite-reduced UndA protein (1 mM total iron) were frozen in liquid N_2 for XAS measurements. X-ray absorption spectra were collected at beamline 7-3 at the Stanford Synchrotron Radiation Lightsource, operating under ring conditions of 500 mA and 3 GeV. A Si(220) monochromator ($\varphi = 90°$) was used for energy selection of the incident beam, and harmonic rejection was achieved through detuning the monochromator by 50% and 97.5% for the dithionite-reduced and aerobically isolated samples, respectively. The energy of the beam was calibrated using the first inflection point of an Fe foil located upstream of the sample. The sample was placed at 45° with respect to the incident

beam, and the iron Kα fluorescence was collected via a 30-element germanium detector. Beam intensity was monitored using an N_2-filled ion chamber placed before the sample. The sample temperature was maintained at 10 K using a Displex closed circle cryostat.

Data processing was carried out in the EXAFSPAK software package.[3] The pre-edge background was subtracted using a Gaussian function, and three-segment splines (of orders 2, 3, and 3) were used to subtract the background from the EXAFS region (in PySpline[4]). The EXAFS were then fit using OPT. Scattering paths for EXAFS fitting were generated using FEFF 9.0[5] using partially optimized crystallographic coordinates described in the next section, modified to move Fe2 to a distance of 3.4 Å from Fe1 in an effort to better represent a typical diiron cluster. Paths generated from an additional model where the Fe-Fe distance was 4.0 Å did not significantly improve the fit of the data for the as-isolated sample. During EXAFS fitting, the distance, Debye-Waller factors, and the E_0 parameter were allowed to float, while the coordination numbers were systematically varied.

Crystallization and structure determination of Fe-soaked UndA. In an anoxic chamber, 10 mg/mL O_2-free apo-UndA, purified as described above, was incubated for 15 min with 5 mM LA in 50 mM sodium 2-[4-(2-hydroxyethyl)piperazin-1-yl]ethanesulfonic acid (HEPES) buffer (pH 7.5) containing 10% glycerol. The sample was mixed with 0.5 volume equiv of a precipitant solution [0.1 M MES, pH 6.5, 10% dioxane, 1.8 M $(NH_4)_2SO_4$] in hanging-drop vapor-diffusion trials. The resulting crystals were soaked for 4-5 h at 25 °C by addition to crystal drops of an equal volume of 10 mM $(NH_4)_2Fe(SO_4)_2$ dissolved in the crystallization solution. Fe(II)-soaked crystals were cryoprotected in well solution supplemented with 20% (*v/v*) glycerol, mounted on rayon loops, and flash freezing by direct plunge into liquid nitrogen.

All crystallographic datasets were collected at beamlines of the Advanced Photon Source at Argonne National Laboratory, and the diffraction images were processed with the software package HKL2000.[6] The native crystallographic dataset was collected at the LS-CAT 21ID-G beamline equipped with a MAR CCD 300 detector. The anomalous diffraction dataset was collected at the GM-CA 23ID-D beamline by using a Pilatus 16M detector. UndA crystallizes in the $P222_1$ space group with two molecules in the asymmetric unit. Phase information was obtained by molecular replacement using PHASER[7] implemented within the CCP4 suite[8] with the published UndA structure (PDB accession code 4WWJ) as the initial search model. Initial refinements in

Refmac5[9] were followed by rounds of manual model building in COOT.[10] Final refinements were carried out in Phenix.[11] A summary of data collection and refinement statistics can be found in Table S2. Figures were generated with the PyMOL molecular graphics software package (Schrödinger, LLC). The final model contains residues 3-195 and 199-257 in chain A; residues 4-7, 9-195, and 200-247 in chain B; two lauric acid (DAO) substrate molecules; four Fe(II) ions; 250 water molecules; and one glycerol molecule. Model analysis with the Molprobity server[12] indicated that 99% of residues lie in favorable regions of the Ramachandran plot, with the remaining 1% in additionally allowed conformations. The structure exhibits a Molprobity score of 0.82 (100th percentile).

Detection by gas chromatography – mass spectrometry (GC-MS) of 1-undecene produced by cultures over-expressing UndA variants. Cultures of *Ec* BL21 star transformed by the plasmid vectors encoding UndA ligand variants were grown in 3 mL of LB medium for ~12 h at 37°C. A 300 µL aliquot of this culture was used to inoculate 30 mL of TB media supplemented with 0.5% glycerol, 1 mM ascorbic acid, 200 µM lauric acid, and appropriate antibiotics in a shake flask. Once the OD_{600} reached ~ 0.6, the culture was cooled on ice for 10 min and then induced by 0.1 mM IPTG. A 1.5 mL aliquot of the culture was shaken in a sealed 20 mL vial containing a stir bar at 30 °C for 36 h. 1-Undecene was detected as previously described.[1] Protein purification and SDS-PAGE analysis were also performed, as described previously,[1] to verify protein over-expression.

Stopped-flow absorption spectroscopy (SF-Abs) and data analysis. SF-Abs experiments were carried out at 5 °C on an Applied Photophysics Ltd. (Leatherhead, UK) SX20 stopped-flow spectrophotometer housed in an anoxic chamber (Labmaster, MBraun, Stratham, USA). The instrument was configured for single-mixing, an optical path length of 1 cm, and data acquisition with a photodiode-array (PDA) detector. Time-dependent absorption spectra (1000) were acquired in a logarithmic time base. An O_2-free solution of apo-UndA (0.30 mM), 0.54 mM $(NH_4)_2Fe(SO_4)_2 \cdot 6H_2O$, 1.0 mM lauric acid (LA), and 1% tergitol NP-40 was rapidly mixed with an equal volume of O_2-saturated (~ 1.8 mM at 5 °C) buffer (50 mM Tris-HCl, pH 8.5, containing 300 mM NaCl and 10 % glycerol). Minor deviations from these reaction conditions are indicated in the appropriate figure legends. To resolve the kinetics of tyrosyl radical species from absorbance

changes contributed by other intermediates, the previously described dropline approach was used.[13]

Preparation of freeze-quenched samples. General procedures for single-mixing freeze-quench EPR and Mössbauer experiments have been published previously.[14-16] UndA purified from *Ec* cultured in M9 minimal medium supplemented with 50 μM $^{57}Fe(SO_4)_2$ at inoculation and 50 μM additional $^{57}Fe(SO_4)_2$ at induction retained 0.5 equiv ^{57}Fe(III) through the aerobic purification. This preparation was reduced to the ^{57}Fe(II)-containing form by incubation at 4 °C in the absence of O_2 with 10 mM sodium dithionite for 30 min. To increase ^{57}Fe(II) occupancy, 1.5 equiv additional $^{57}Fe(SO_4)_2$ was added, and the protein was incubated for for an additional 30 min. The sodium dithionite and excess ^{57}Fe(II) were removed by passage through a PD-10 desalting column (G-25 Sephadex medium, GE Healthcare) in O_2-free lysis buffer. In preparing freeze-quench Mössbauer samples, an O_2-free solution containing the ^{57}Fe(II)-UndA (1.2 mM), 10 mM LA and 1.2% tergitol NP-40 was mixed at 5 °C with an equal volume of O_2-saturated (1.8 mM O_2) 50 mM Tris-HCl (pH 8.5) buffer containing 300 mM NaCl and 10% glycerol. The resultant solution was rapidly frozen (freeze-quenched) in isopentane at -150 °C after varying reaction time. In preparing freeze-quench EPR samples, an O_2-free solution containing 1.1 mM wild-type apo-UndA (from over-expression in LB medium), 2.2 mM $^{57}Fe(SO_4)$, 3.6 mM LA and 1% tergitol NP-40 was mixed at 5 °C with an equal volume of O_2-saturated (1.8 mM O_2) 50 mM Tris-HCl (pH 8.5) buffer containing 300 mM NaCl and 10% glycerol. The resultant solution was rapidly frozen (freeze-quenched) in isopentane at -150 °C after varying reaction times. Minor deviations from these experimental procedures are noted in the appropriate text and figure legends.

UndA activity assays. Single-turnover assays monitoring lauric acid consumption were conducted inside an anoxic chamber (Labmaster, MBraun, Stratham, USA). For assays with excess substrate and Fe(II), a solution (0.1 mL) containing 0.4 mM wild-type or W190F apo-UndA, 0.8 mM $(NH_4)_2Fe(SO_4)_2$, 0.8 mM lauric acid, and 0.5% tergitol NP-40 was mixed with an equal volume of O_2-saturated (~ 1.8 mM O_2 at 5 °C) buffer (100 mM Tris-HCl, pH 8.5, 300 mM NaCl) and incubated for 5 min at ambient temperature. Assays examining substrate consumption as a function of Fe(II):UndA were carried out as described above but with 0.6 mM lauric acid (prior to mixing) and varying concentration of $(NH_4)_2Fe(SO_4)_2$ in the protein reactant solution; these reactions were

incubated for 2 min at ambient temperature. All reactions were quenched with 0.04 mL saturated NH_4OH solution then boiled for 5 min, and 0.012 mL 2 mM octanoic acid was added as internal standard. Reaction solutions were then filtered through a centrifugal device with 10 kDa molecular weight cutoff (Pall Corporation) prior to HPLC-MS analysis.

High performance liquid chromatography – mass spectrometry (HPLC-MS) analysis. HPLC-MS of reaction samples was carried out on a 1260 series LC system coupled to a 6460 series triple quadrupole mass spectrometer (Agilent Technologies, Santa Clara, CA). The associated Agilent MassHunter software package was used for data collection and analysis. Quenched, filtered reaction solutions (2 μL) were injected on an Agilent Zorbax Extend-C18 column (4.6 x 50 mm, 1.8 μm particle size) in 95% solvent A (99:1 H_2O:saturated NH_4OH solution) and 5% solvent B (CH_3CN). The column was developed at a flow rate of 0.5 mL/min. Chromatographic separation was achieved with a 5-min gradient of 95-5% solvent A. A 2-min gradient of 5-95% solvent A and 3 min wash at 95% solvent A prepared the column for the next injection. The substrate were detected by electrospray ionization (ESI-MS) in the negative mode (source parameters: gas temperature = 300 °C, gas flow = 5 L/min, nebulizer pressure = 45 psi, capillary voltage = 3500 V) with single ion monitoring at 199 *m/z* (fragmentor voltage = 90 V, cell accelerator voltage = 7 V, dwell time = 0.2 s, delta EMV = 0 V). Substrate concentration was determined by comparison to an external standard curve of varying LA.

Spectroscopic evidence for a diiron cofactor in UndA

Mössbauer-spectroscopic evidence for a Fe_2(III/III) cluster in Pseudomonas fluorescens Pf-5 *UndA*. The Fe-containing cofactor in *Pseudomonas fluorescens* Pf-5 UndA was first examined by ^{57}Fe Mössbauer spectroscopy, which provides information on the nature of all Fe species in a sample. Consistent with the report by Manley, *et al.*,[17] the 4.2-K/53-mT Mössbauer spectrum of the aerobically isolated UndA from minimal media supplemented with ^{57}Fe (described above) is dominated by a quadrupole doublet feature with isomer shift (δ) of 0.51 mm/s and quadrupole splitting (ΔE_Q) of 0.65 mm/s (**Figure S2**, *top*, *vertical bars*). The isomer shift is characteristic of a N/O-coordinated high-spin (S = 5/2) Fe(III) ion. Importantly, the fact that the majority of the ^{57}Fe-containing species (~ 90% of total ^{57}Fe absorption) gives rise to a quadrupole doublet feature at 4.2 K in the presence of a weak magnetic field implies that the predominant iron species in as-

purified UndA has an integer-spin electronic ground state resulting from antiferromagnetic (AF) coupling of two high-spin Fe(III) ions in a Fe_2(III/III) cluster. Whereas the individual doublets of the two Fe(III) sites in as-purified *Pseudomonas fluorescens* Pf-5 UndA are, unlike those in the *P. syrinae pv. tomato* DC3000 UndA,[17] not resolved, the isomer shift value is identical and the magnitude of the quadrupole splitting is similar to the average value of the two Fe(III) sites in that orthologue. The sample also contained a small amount (~10 % of total ^{57}Fe absorption) of mononuclear Fe(III) species, as evidenced by the Mössbauer spectra recorded in strong magnetic fields of 4 and 8 T (**Figure S2**, *middle and bottom*, *vertical bars*), where the spectral contribution of mononuclear high-spin Fe(III) is better resolved due to the strong Zeeman effect (**Figure S2**, *blue lines*). The small quantity of mononuclear Fe(III) species likely results from incomplete occupancy of one of the iron sites. In the high-field spectra, the central portion of the spectrum is associated with the Fe_2(III/III) cluster. Simulations assuming values for δ and ΔE_Q obtained from the 53-mT spectrum and assuming a $S = 0$ ground state are shown as red lines. The deviation between the simulation and experiment (*arrows*) result from antisymmetric exchange interaction, as was also reported for the Fe_2(III/III) form of *P. syrinae pv. tomato* DC3000 UndA,[17] the Fe_2(III/III) cluster in soluble methane monooxygenase hydroxylase,[citation] and an inorganic Fe_2(III/III) complex.[18]

Fe K-edge EXAFS evidence for a diiron cofactor in UndA. The aerobically isolated and sodium dithionite-reduced forms of UndA were analyzed by extended X-ray absorption fine structure (EXAFS). The data from the Fe K-edge region (**Figure S3**, *left*) were fit according to the parameters given in **Table S3**. The Fourier transform of the EXAFS data for the aerobically isolated UndA sample (**Figure S3**, *right*) exhibits a strong scatterer at R+Δ ~ 2.6. This feature arises from an Fe-Fe scattering vector at a distance of 3.21 Å, consistent with two iron ions in a Fe_2(III/III) cluster.[19-23] Alternative fits replacing the single Fe-Fe scattering vector were considered; however, neither additional Fe-C/N/O scatterers nor two Fe-Fe scatterers produced superior fits (**Figure S4)**. Other components of the overall fit include three shells of light-atom scatterers at 1.86, 2.10, and 2.57 Å, which are consistent with a (hydr)oxo bridge between the two iron centers, typical His/Glu/Asp coordination, and carbons of the ligand residues, respectively. In the Fourier transform of the EXAFS data obtained for reduced UndA (**Figure S3**, *right*), the peak corresponding to the Fe-Fe scatterer at 3.21 Å was absent, and, instead, the data are best fit

considering an Fe-Fe scatterer at a distance of 3.97 Å. Although an increase in the Fe-Fe distance is expected for a decrease in the iron oxidation state, this distance is notably longer than those reported for Fe_2(II/II) clusters in other ferritin-like non-heme-diiron enzymes (3.16-3.53 Å).[20,23-24] The unusually large spatial separation of the two Fe centers in the reduced state suggests that the cluster may not have a single-atom bridging ligand.

X-band EPR spectroscopic-evidence for a mixed-valent Fe_2(II/III) cluster in UndA. The aerobically isolated protein and reduced forms were probed by EPR spectroscopy (**Figure S5**). In the aerobically isolated protein, the major Fe_2(III/III) species is EPR-silent, as expected, while the minor mononuclear high-spin Fe(III) species gives rise to the characteristic signal at g_{eff} = 4.3 (**Figure S5,** *top spectrum*). Partial reduction of the aerobically isolated UndA with a sub-stoichiometric quantity of sodium dithionite (0.5 electrons/Fe) resulted in the development of a signal with principal *g*-values < 2, indicative of a S_{total} = 1/2 electronic ground state of an antiferromagnetically coupled mixed-valent Fe_2(II/III) cluster (**Figure S5,** *middle spectrum*). Similar EPR signals have been observed in several other nonheme diiron proteins.[25-27] Accumulation of this state to ~ 10% in UndA further supports the presence of a coupled diiron cluster. The EPR signal of the Fe_2(II/III) UndA disappears upon addition of excess sodium dithionite, suggesting complete reduction of the diiron cluster (**Figure S5,** *bottom spectrum*). The sharp signal in the center is due to the presence of methyl viologen (100 μM) as a redox mediator.

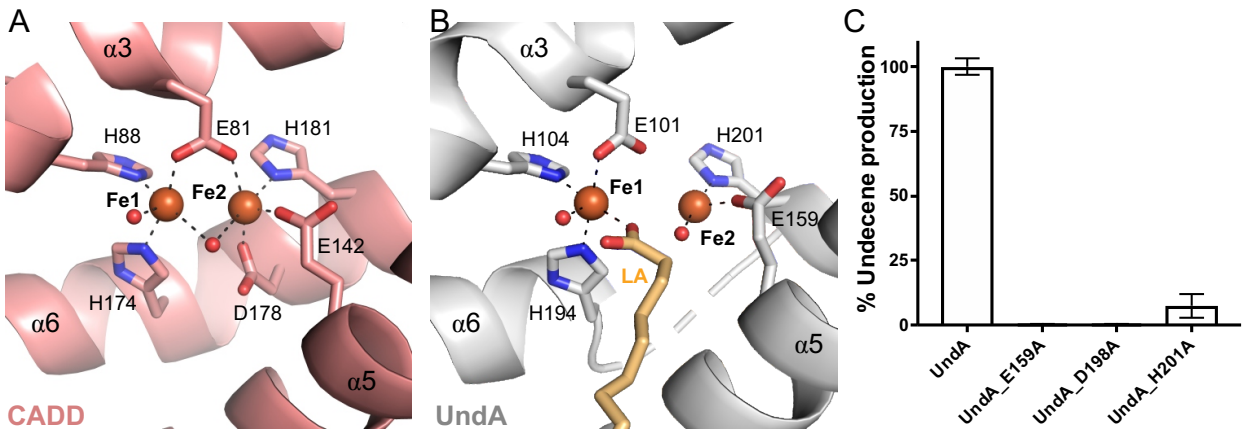

D

	helix 3		helix 5		helix 6			
	101	104	159		190	194	198	201
UndA	**E**L-------N**H**ADYW		VAIAATNYAI**E**GATGE		**W**LKM**H**AQY**D**DA**H**PWEALEII			
CADD	**E**E---NGYPN**H**IDLW		AGVAAL-YSY**E**SQIPR		**Y**FTE**H**EEA**D**VR**H**AREEKALI			
SznF	**E**YGYGVHDTK**H**STLF		RYVGAL-YYT**E**SSLVD		**Y**FTE**H**IHI**D**QH**H**GRMAREKI			
BesC	**E**V---GSDPT**H**STLF		KALGAL-YAD**E**TMSSI		**F**WQL**H**IDV**E**VG**H**SNSVFNAI			

Figure S1. Predicted, conserved amino acid ligands for Fe2 are essential for 1-undecene production. A depiction of the first coordination sphere of the diiron cofactors in (***A***) CADD (PDB accession code 1RCW) and (***B***) UndA (PDB accession code 6P5Q). Ligand D198 in UndA is missing due to persistent disorder in helix 6 in the current crystallographic model of the diiron form of the enzyme. (***C***) 1-Undecene production in cultures of *Ec* over-expressing wild-type or variant UndA proteins. (***D***) Alignment of amino acids in the ligand-contributing helices of diiron HO-like oxidases and oxygenases with predicted coordinating residues highlighted in bold. In helix 6, a conserved aromatic amino acid near site 1 (W190 in UndA, a side chain that mediates off-pathway Tyr• accumulation) is also indicated.

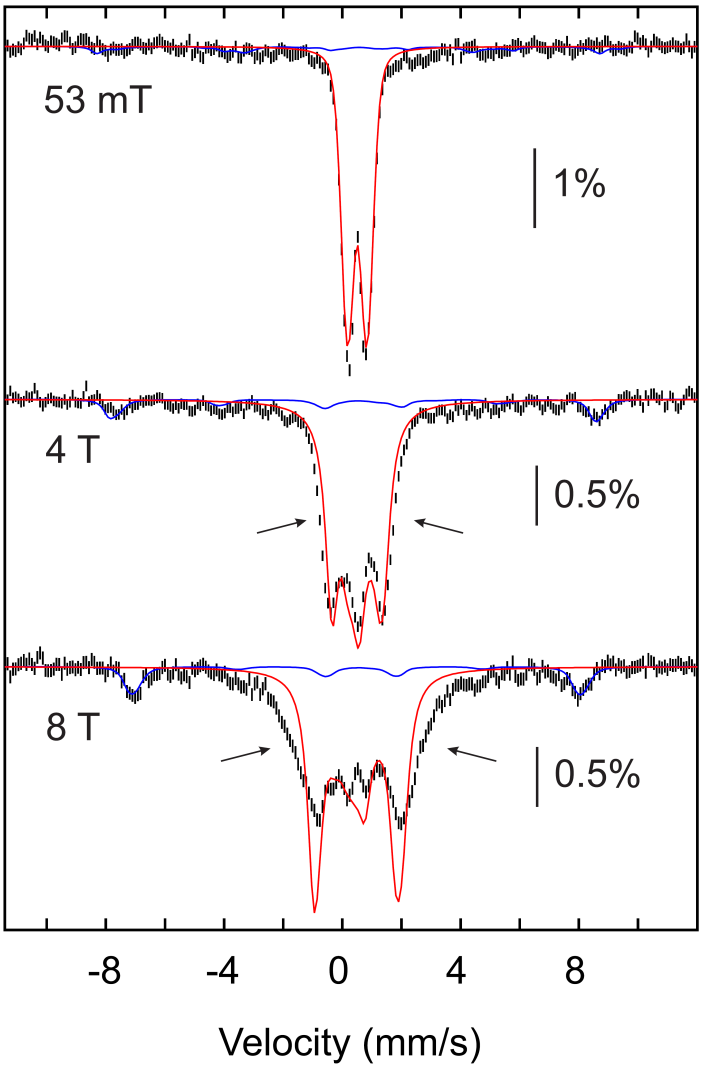

Figure S2. 4.2-K Mössbauer spectra (black vertical bars) of the ^{57}Fe-enriched, aerobically-isolated UndA protein measured with applied fields of 53 mT, 4 T and 8 T oriented parallel to the γ beam. Simulations of the spectra of the mononuclear Fe(III) (*blue lines*) assumed $S = 5/2$, $g_{5/2,iso} = 2.0$, $D_{5/2} = 0.5$ cm^{-1}, $(E/D)_{5/2} = 0.33$, $\delta = 0.55$ mm/s, $\Delta E_Q = 0.8$ mm/s, $\eta = 1$, $A/g_N\beta_{N,iso} = -22$ T. Simulations of the spectrum of the Fe_2(III/III) cluster (*red lines*) assumed $S = 0$, $\delta = 0.51$ mm/s, $\Delta E_Q = 0.65$ mm/s, $\eta = 0$. The arrows indicate deviation between the simulation and experiment resulting from antisymmetric exchange interaction.

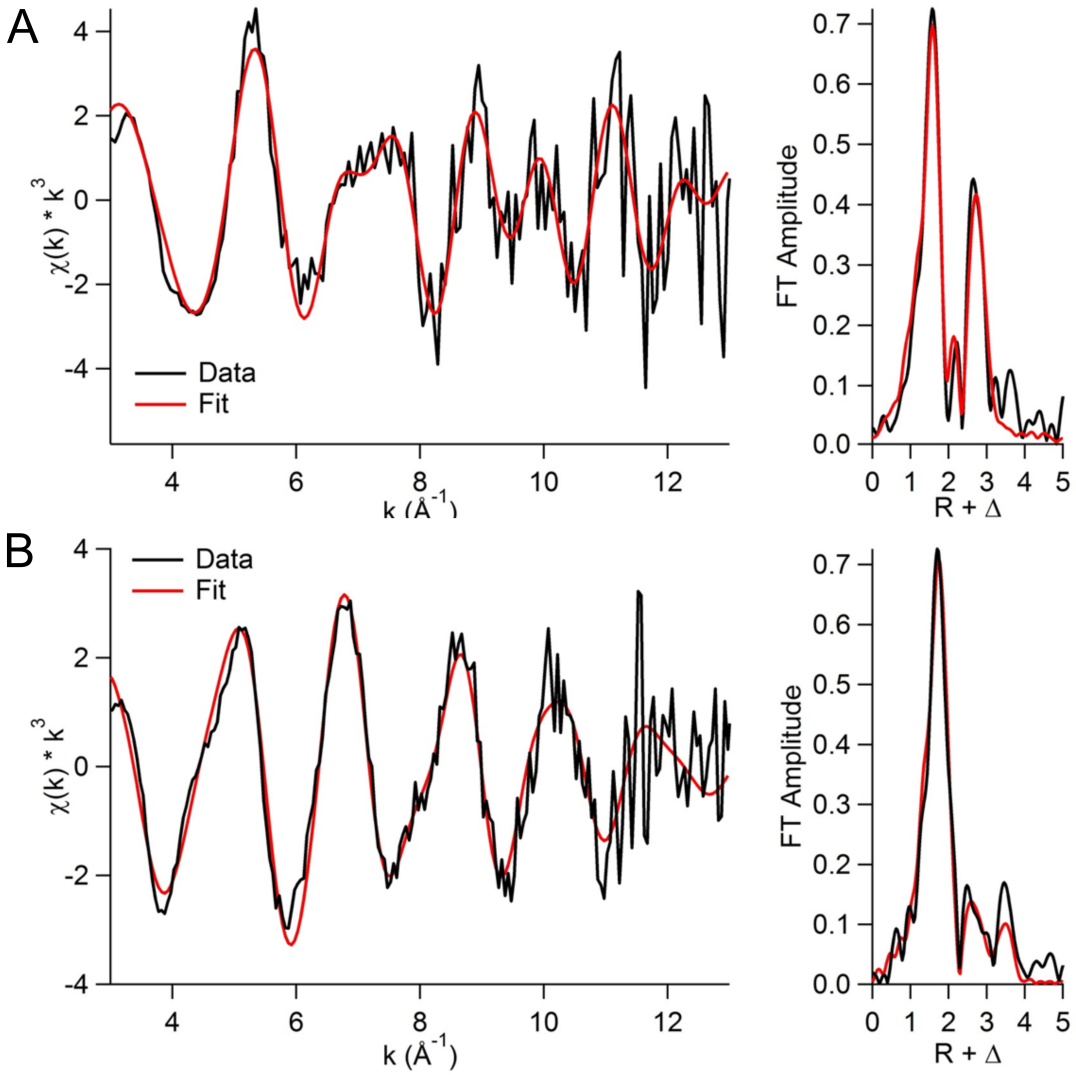

Figure S3. Fe-K-edge EXAFS data (*left*) and Fourier transforms (*right*) for samples of aerobically isolated UndA before (***A***) and after (***B***) reduction with 10 mM sodium dithionite. The parameters of the fits (*red lines*) are provided in Table S3.

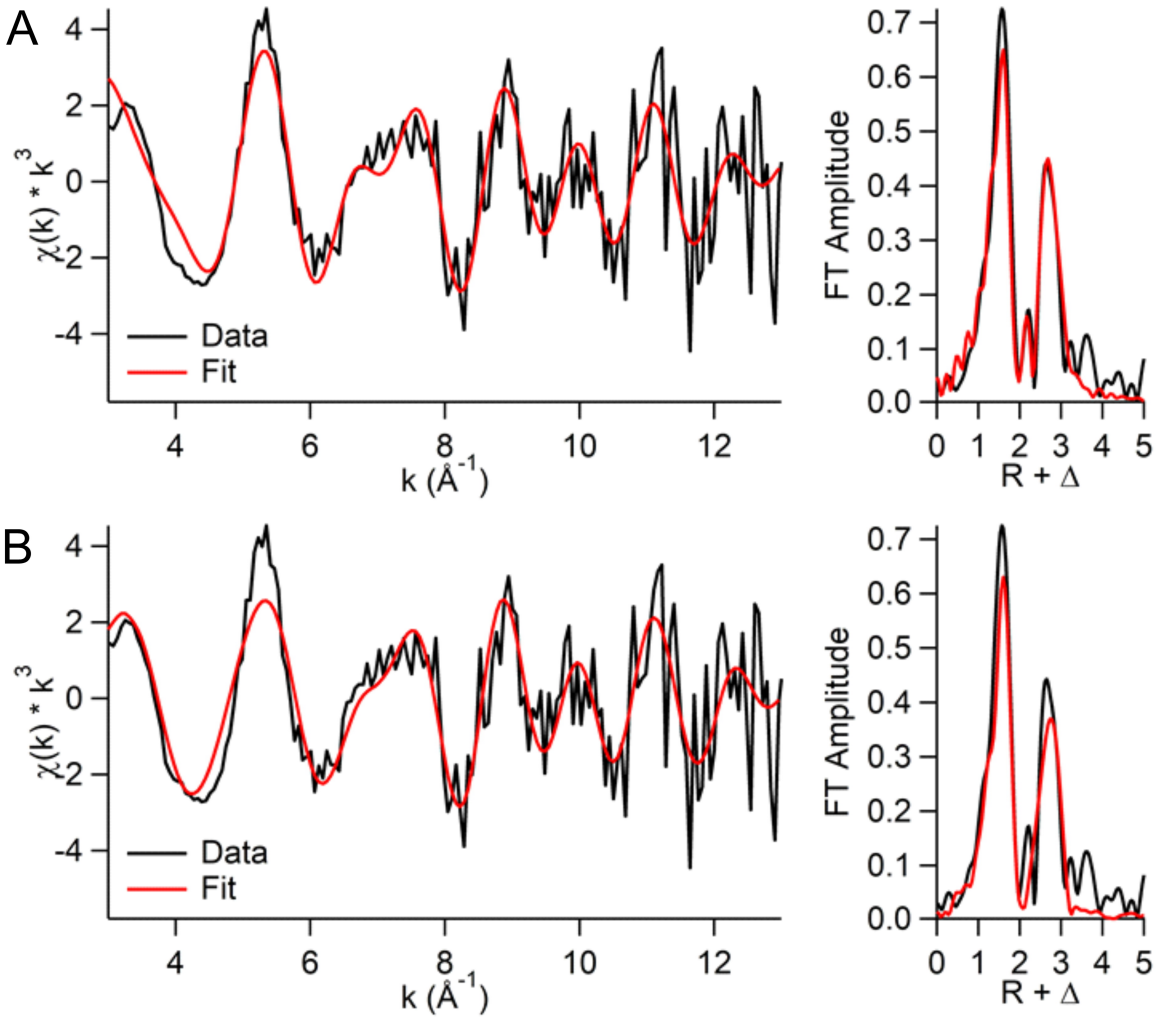

Figure S4. Alternative fits to the Fe-K-edge EXAFS data (*left*) and Fourier transforms (*right*) for aerobically isolated UndA where (***A***) no Fe-Fe vector is included and (***B***) two separate M-M vectors are considered. The parameters of the fits (*red*) are provided in Table S4.

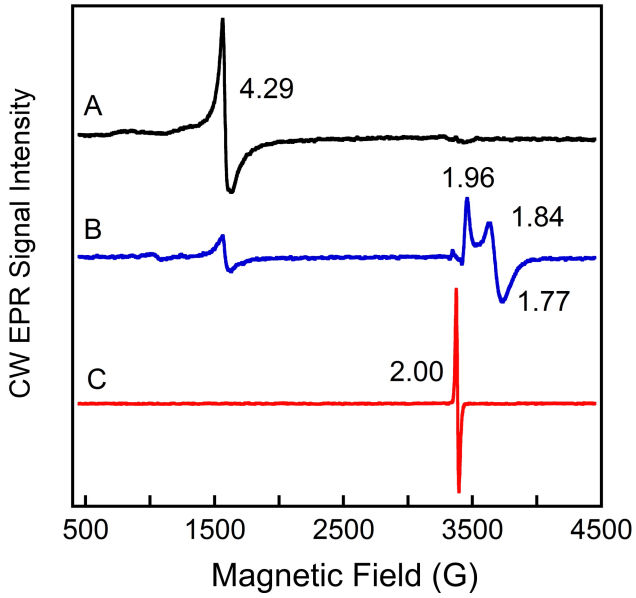

Figure S5. X-band EPR spectra of UndA protein isolated aerobically from Fe-supplemented M9 growth media (0.3 mM diiron cofactor) untreated (***A***) or treated with 0.5 (***B***) or 1.5 (***C***) reducing equivalents per diiron cofactor, delivered by sodium dithionite in the presence of 0.1 mM of the redox mediator, methyl viologen. Experimental conditions: temperature = 9.5 K, microwave power = 0.2 mW (2 μW for *C*), microwave frequency = 9.480 GHz, modulation amplitude = 1 mT.

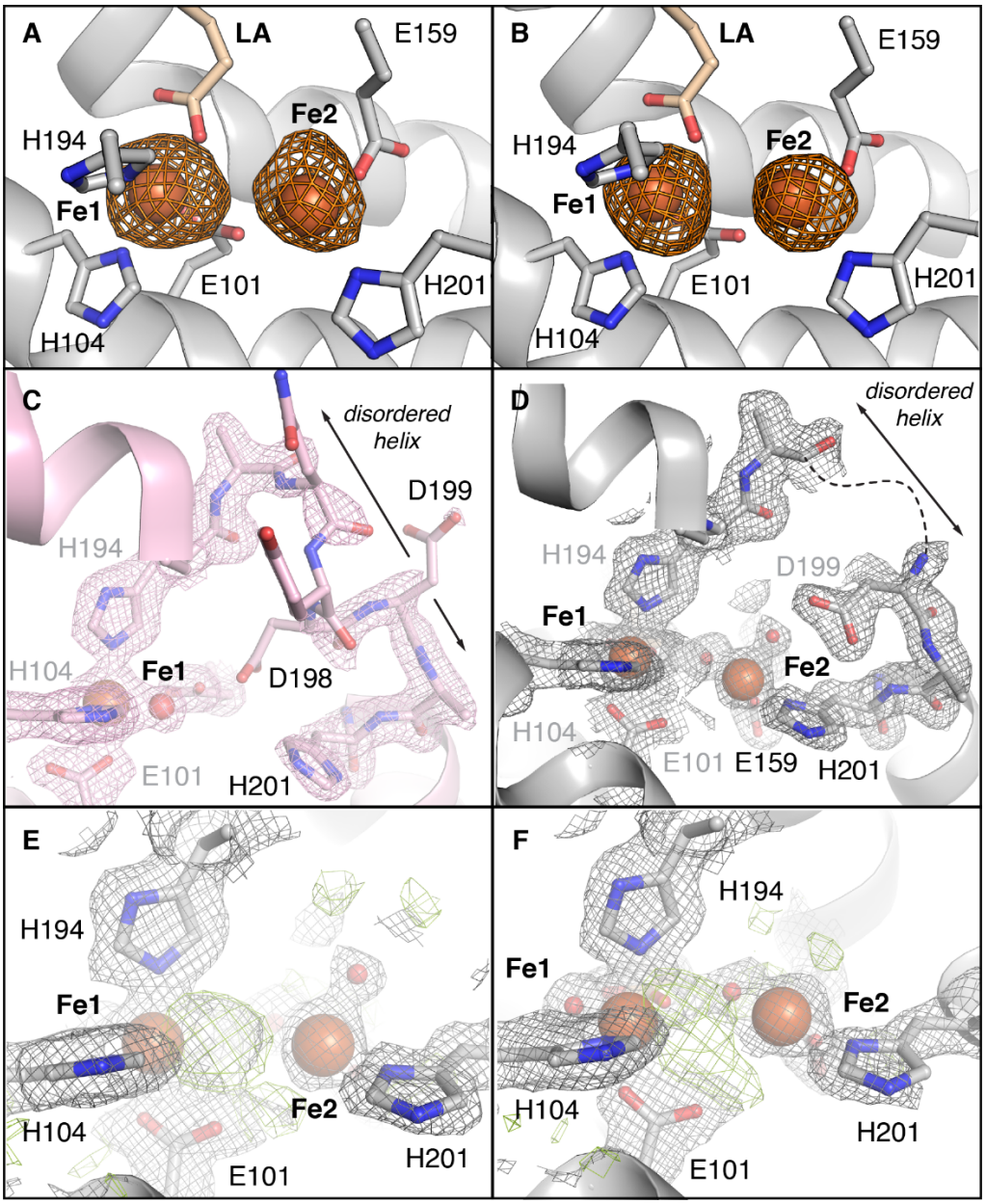

Figure S6. Soak of Fe(II) into pre-formed UndA crystals increases the metal ion occupancy of site 2 but fails to order all of the corresponding ligands. Anomalous difference maps (*orange mesh*, contoured at 3.0σ) collected above the iron *K*-edge x-ray absorption peak energy (7.2 keV) are shown for the active site in chain A (***A***) and chain B (***B***). The anomalous map peak heights for site 1 are consistently higher (20σ in chain A, 17σ in chain B) than those for site 2 (14σ in chain A, 11σ in chain B). Occupancy refinement of each site yields nearly full population of site 1 (90-100%) in both chains but variable occupancy of site 2 (95% chain A, 55% chain B). In the original

x-ray structures of *P. fluorescens Pf-5* UndA (PDB accession code 4WWJ), a helix containing proposed ligands (H201, D198) to the site 2 metal ion exhibits weak $2F_o$-F_c electron density (pink mesh, contoured at 1.5σ) for backbone atoms and little basis for modelling the carboxylate side chain (***C***). The corresponding region in the soaked diiron structure remains disordered, (***D***) even at a lower $2F_o$-F_c map contour (gray mesh, 1.0σ). The side chain of D199 becomes visible near the site 2 Fe^{II} ion, but neither Y197 nor D198 can be modeled with confidence. Residue D198 is essential for enzyme activity and conserved in other structurally characterized heme oxygenase-like diiron proteins (Figure S1).[28-29] Therefore, we conclude that D199 is not a metal ligand. Instead, D198 is likely a site 2 ligand, even though it is not visualized in the current crystallographic dataset. Additional unmodeled electron density can be observed in the $2F_o$-F_c (*gray mesh*, 1.0σ) and F_o-F_c (*green mesh*, 3.0σ) maps in chains A (***E***) and B (***F***), consistent with the presence of additional ligands that remain undefined in the crystallographic model as a result of low metal occupancy at site 2. The low metal occupancy at site 2 and the incomplete first coordination sphere make estimates of the metal-metal and metal-ligand distances of this structural model uncertain.

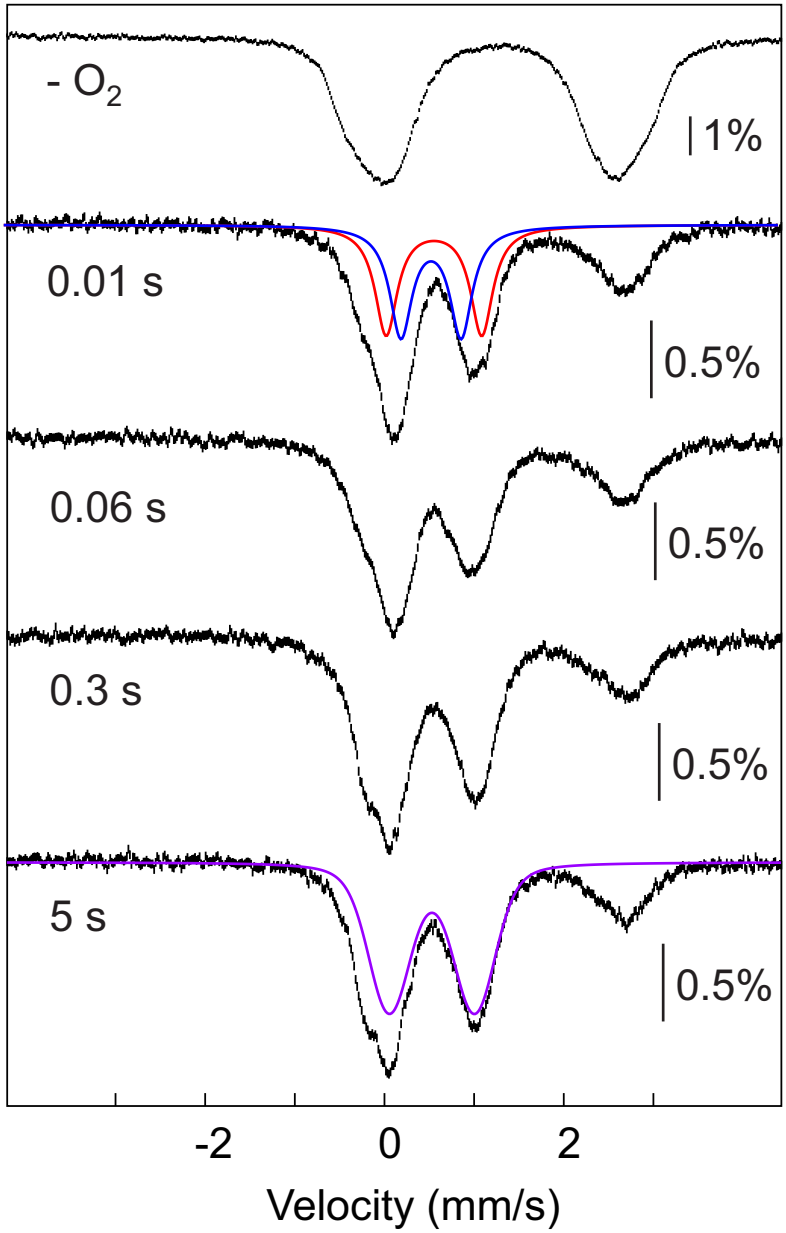

Figure S7. 4.2-K/53-mT Mössbauer spectra (vertical bars) of samples obtained by mixing a solution containing 1.4 mM UndA, 2.0 mM ^{57}Fe(II) (prepared as described in the *Experimental Section*), and 10 mM LA with an equal volume of O_2-saturated buffer (~1.8 mM O_2) at 5 °C and freeze-quenching after the reaction times indicated in the figure. The solid lines are simulations of the spectra of the peroxo-Fe_2(III/III) intermediate (*red and blue*) and Fe_2(III/III) product complex (*purple*) generated with parameters quoted in the main text.

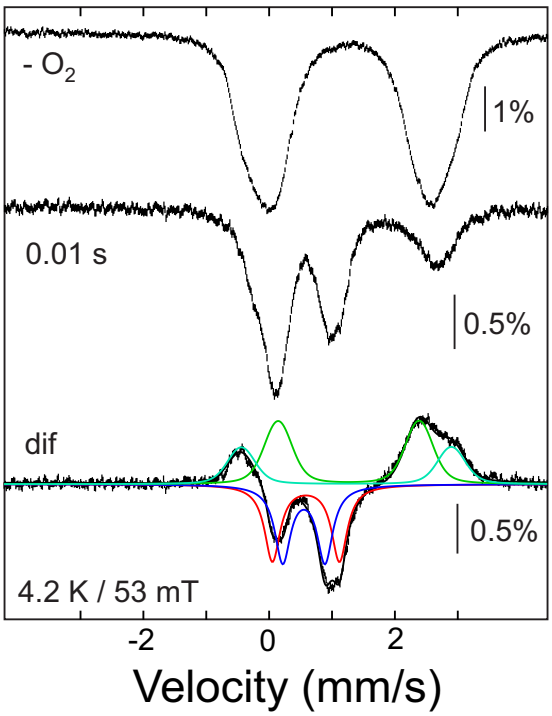

Figure S8. Determination of the Mössbauer parameters of the peroxo-Fe_2(III/III) intermediate. Experimental 4.2-K/53-mT Mössbauer spectra of the reactant solution (- O_2, *top*) and the 0.01-s sample (*middle*) are shown as vertical bars. In the experimental [0.01s – (- O_2)] difference spectrum (*bottom*, vertical bars), the features pointing upward correspond to the spectrum of the O_2-reactive Fe_2(II/II) complex, while the features pointing downward arise from the peroxo-Fe_2(III/III) intermediate . The high-energy line region of the Fe(II) species (~ 2.4 mm/s, pointing upwards) exhibits marked asymmetry, suggesting the presence of at least two distinct reactant complexes. Likewise, the high-energy line of the intermediate (~ 1.0 mm/s, pointing downwards) is also partially resolved, suggesting two distinct sites. Therefore, the difference spectrum was simulated with four quadrupole doublets. In order to reduce the number of variables, we assumed (i) that the peroxo-Fe_2(III/III) complex has two distinct sites, each giving rise to a quadrupole doublet with equal intensity and equal line width [δ_1 = 0.59 mm/s, $|\Delta E_Q|_1$ = 1.07 mm/s, Γ_1 = 0.35 mm/s, 30% intensity (*red line*) and δ_2 = 0.56 mm/s, $|\Delta E_Q|_2$ = 0.67 mm/s, Γ_2 = 0.35 mm/s, 30% intensity (*blue line*)] and (ii) that the O_2-reactive fraction of the Fe(II) species can be modeled with two symmetrical quadrupole doublets with equal line width [δ_3 = 1.28 mm/s, $|\Delta E_Q|_3$ = 2.20 mm/s, Γ_3 = -0.61 mm/s, 38% intensity (*green line*) and δ_4 = 1.24 mm/s, $|\Delta E_Q|_4$ = 3.31 mm/s, Γ_4 = mm/s, 23% intensity (*cyan line*)]. The positive or negative signs of the linewidth indicate a Lorentzian or Voigt line shape, respectively.

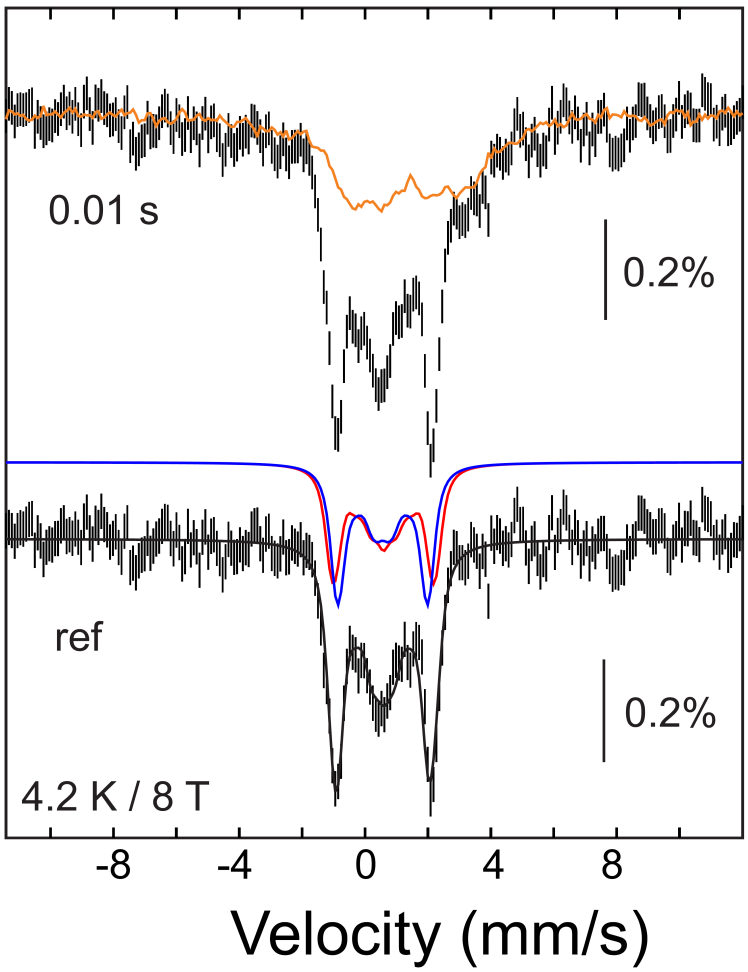

Figure S9. 4.2-K/8-T Mössbauer spectra of the 0.01-s sample described in the main text **Figure 2** (*top*, vertical bars) and of the O_2-free control sample (*top*, orange solid line, scaled to 40% of the total intensity of the spectrum of the 0.01-s sample). Subtraction of the spectrum of the reactant complex yields the experimental reference spectrum of the peroxo-Fe_2(III/III) intermediate (*bottom*, vertical bars), which can be simulated with two sites using the following parameters and assuming a diamagnetic ($S = 0$) ground state (δ and ΔE_Q were fixed to values obtained from analysis of the 53-mT spectrum): $\delta_1 = 0.59$ mm/s, $\Delta E_{Q1} = 1.07$ mm/s, $\eta_1 = 0$, $\Gamma_1 = 0.35$ mm/s, 30% intensity (red line) and $\delta_2 = 0.56$ mm/s, $\Delta E_{Q2} = 0.67$ mm/s, $\eta_2 = 0$, $\Gamma_2 = 0.35$ mm/s, 30% intensity (blue line). The sum of the two components is shown as a black line.

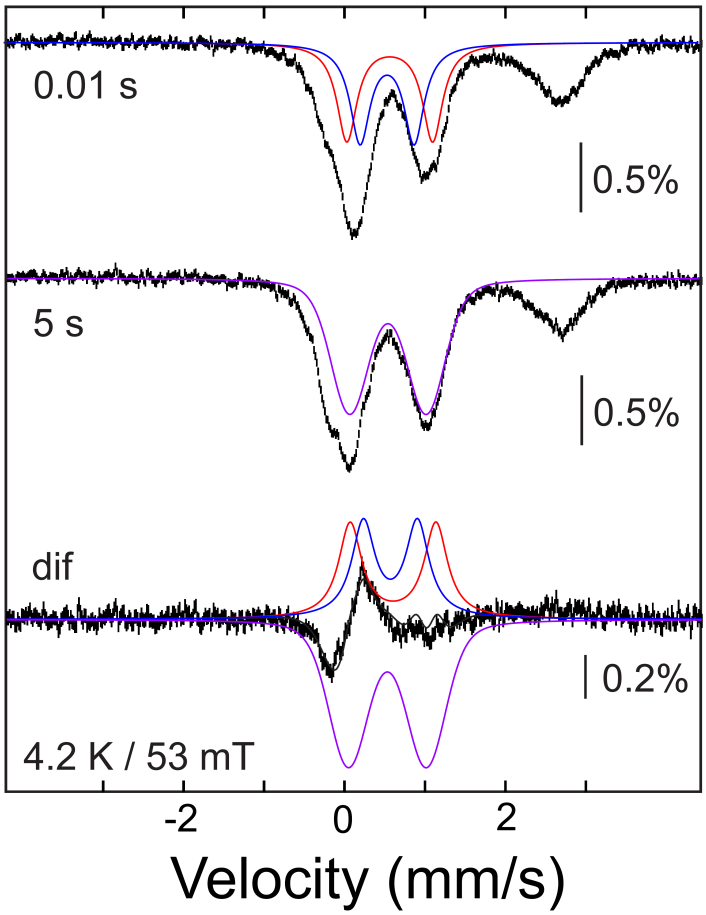

Figure S10. Determination of the Mössbauer parameters of the Fe_2(III/III) product cluster. Experimental 4.2-K/53-mT Mössbauer spectra of the 0.01-s sample (*top*) and the 5-s sample (*middle*) are shown as vertical bars. In the experimental [5s – 0.01s] difference spectrum (*bottom*, vertical bars), the features pointing upward correspond to the spectrum of the peroxo-Fe_2(III/III) intermediate, while those pointing downward correspond to the spectrum of the Fe_2(III/III) product complex. The difference spectrum was simulated with three quadrupole doublets. In order to reduce the number of variables, we assumed (i) that the peroxo-Fe_2(III/III) complex has two distinct sites, each giving rise to a quadrupole doublet with parameters determined from analysis of the [0.01s – 0s] difference spectrum [δ_1 = 0.59 mm/s, $|\Delta E_Q|_1$ = 1.07 mm/s, Γ_1 = 0.35 mm/s, 30% intensity (red line) and δ_2 = 0.56 mm/s, $|\Delta E_Q|_2$ = 0.67 mm/s, Γ_2 = 0.35 mm/s, 30% (blue line), 30% intensity] and (ii) that the diiron(III) can be modeled with one broad symmetrical quadrupole doublet [δ_3 = 0.52 mm/s, $|\Delta E_Q|_3$ = 0.97 mm/s, Γ_3 = -0.57 mm/s, 38% intensity (purple line)]. The positive or negative signs of the linewidth indicate a Lorentzian or Voigt line shape, respectively.

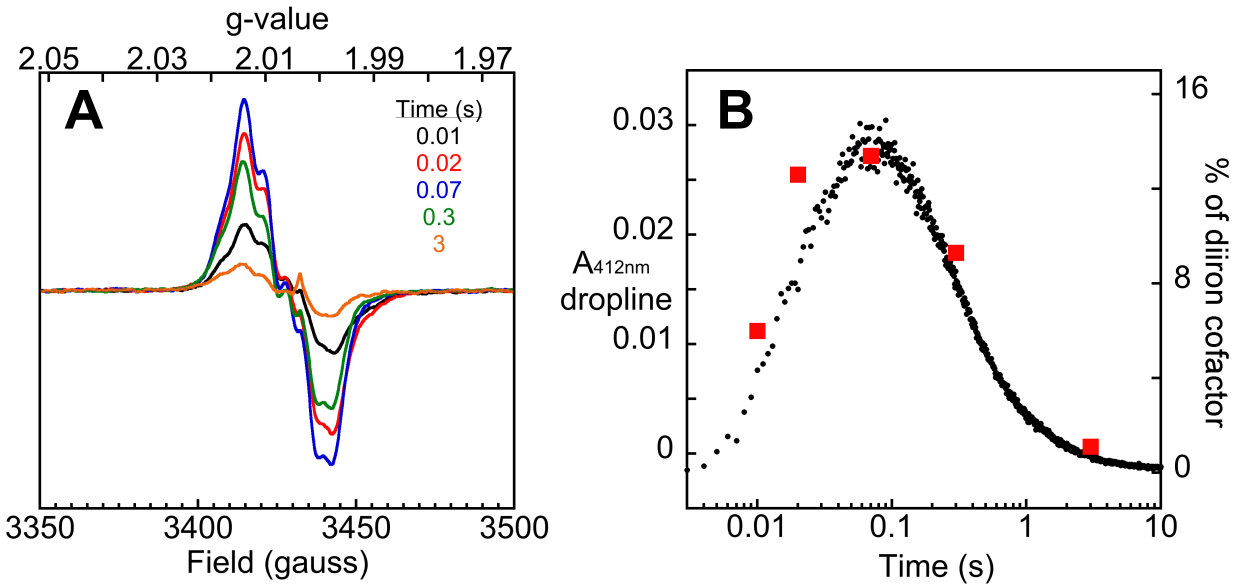

Figure S11. Observation of transient tyrosyl radical species by EPR and UV-visible absorption spectroscopies. (***A***) CW X-band EPR spectra of FQ samples obtained by mixing at 5 °C a solution of 1.2 mM UndA, 2.2 mM Fe(II) and 3.6 mM LA with an equal volume of O_2-saturated buffer (~1.8 mM O_2) and freeze quenching at varying reaction times. Experimental conditions: temperature = 20 K, modulation amplitude = 4 G, microwave frequency = 9.625 GHz, microwave power = 20 μW. (***B***) Comparison of the kinetics of the tyrosyl radical obtained by the dropline analysis [$A_{412nm,dropline} = A_{412nm} - (A_{406nm} + A_{418nm})/2$] with the radical:UndA (in %) determined by spin quantitation relative to a Cu^{2+}-EDTA standard.

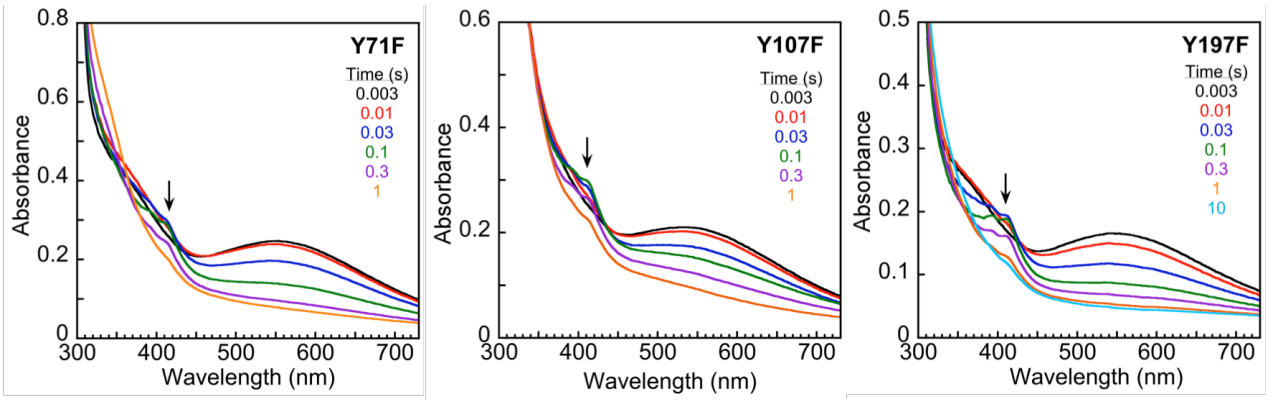

Figure S12. Time-dependent absorption spectra from the reaction of UndA Tyr → Phe variants with O_2. All reactions were carried out by mixing a solution containing 0.3 mM UndA, 0.54 mM Fe(II), and 1.0 mM LA with an equal volume of O_2-saturated buffer (~1.8 mM O_2) at 5 °C. The arrows indicate the absorption feature characteristic of tyrosyl radicals.

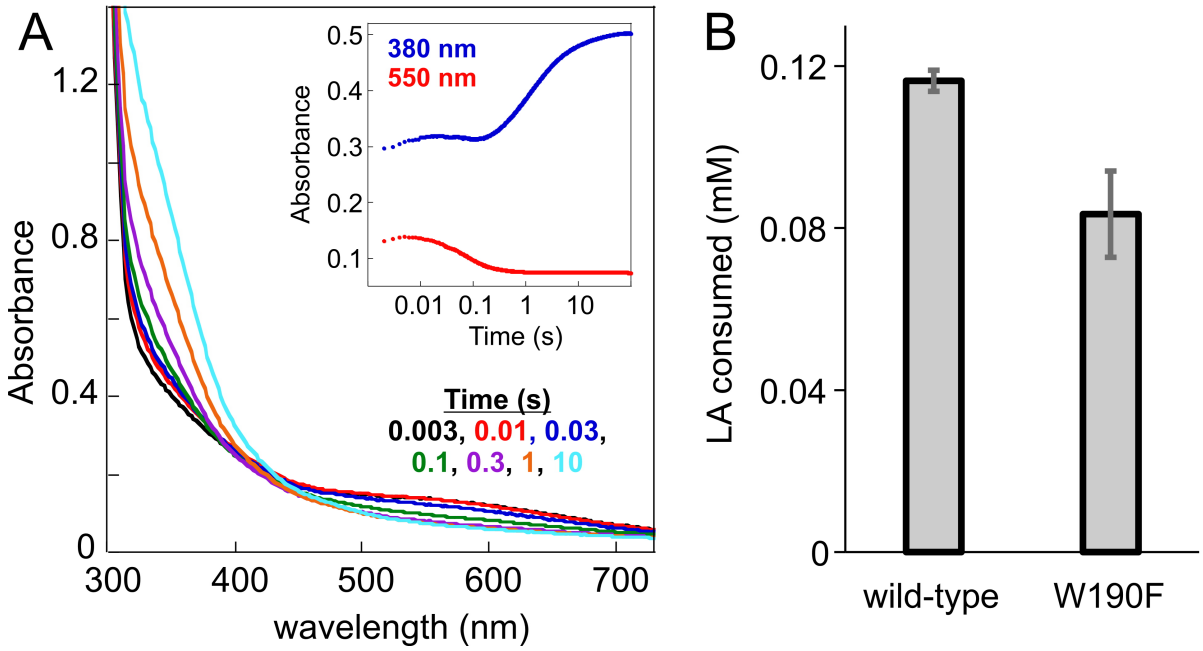

Figure S13. The W190F variant of UndA consumes LA and accumulates the peroxo-Fe_2(III/III) intermediate but fails to accumulate the tyrosyl radical(s). (***A***) Absorption spectra and (*inset*) absorbance versus time traces acquired after rapid mixing of a solution containing 0.6 mM W190F UndA, 1.1 mM Fe(II), and 2.0 mM LA with an equal volume of O_2-saturated buffer (~1.8 mM O_2) at 5 °C. (***B***) Concentrations of LA consumed after mixing a solution of 0.2 mM wild-type or W190F UndA, 0.4 mM Fe(II), and 0.4 mM LA with an equal volume of cold O_2-saturated buffer (~1.8 mM O_2 at 5 °C) and incubating for 5 min at ambient temperature. The absence of the 412-nm absorption feature in the time-dependent spectra indicates that production of the tyrosyl radical species is abolished in the W190F variant. The Fe_2(II/II) complex of W190F reacts rapidly with O_2 in the presence of lauric acid to form the 550 nm-absorbing peroxo-Fe_2(III/III) intermediate, demonstrating that the absence of Tyr• in the W190F variant does not result from unfavorable kinetics (e.g., sluggish reaction with O_2). The slightly diminished efficiency of substrate consumption may result from disrupted binding, as W190 is one of a series of residues that constitute a substrate entry channel and resides in close proximity to one of the Fe ions of the cofactor.

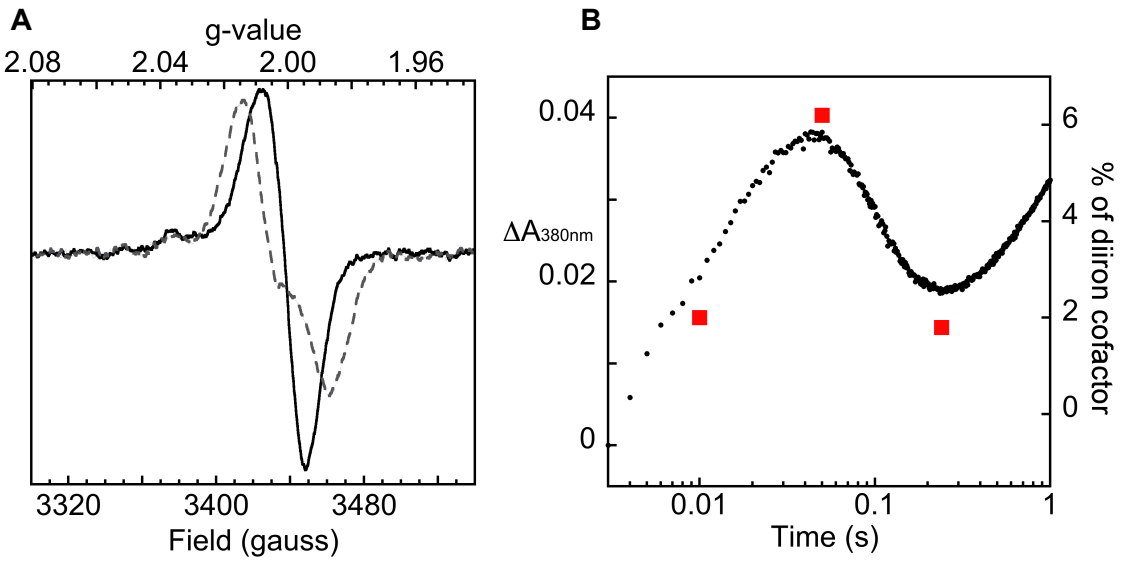

Figure S14. Detection of a transient Fe_2(III/IV) species in the W190F variant of UndA. (***A***) EPR spectra of samples obtained by mixing at 5 °C a solution containing 0.6 mM UndA-W190F, 1.0 mM natural abundance Fe(II) (91.7% ^{56}Fe, $I = 0$) (*solid line*) or ^{57}Fe(II) (*dashed line*) and 6.0 mM per-deuterated LA with an equal volume of O_2-saturated buffer (~ 1.8 mM O_2) and freeze-quenching at 0.05 s. The isotropic EPR signal with $g = 2.001$ is different from that of the tyrosyl radicals (Figure S11A). Its lineshape, ^{57}Fe-hypefine coupling, and magnetic properties identify it as a magnetically isolated Fe_2(III/IV) complex, in which the $S = 2$ high-spin Fe(IV) and $S = 5/2$ high-spin Fe(III) sites are antiferromagnetically coupled to yield an electronic ground state with $S = 1/2$, as observed for the high-valent Fe_2(III/IV) intermediate (X) in class Ia RNR.[30] The presence of this cluster also in the reaction of wild-type UndA is revealed by the subtle ^{57}Fe-induced broadening in the FQ-EPR spectra marked by arrows in Figure S15. The spectrometer conditions were: temperature = 20 K, modulation amplitude = 4 G, microwave frequency = 9.63 GHz, microwave power = 20 mW. (***B***) Comparison of the quantities of Fe_2(III/IV) complex determined by EPR integrations (*red squares*) with the A_{380nm}-versus-time trace from the corresponding SF-Abs experiment (*black points*) carried out under identical conditions.

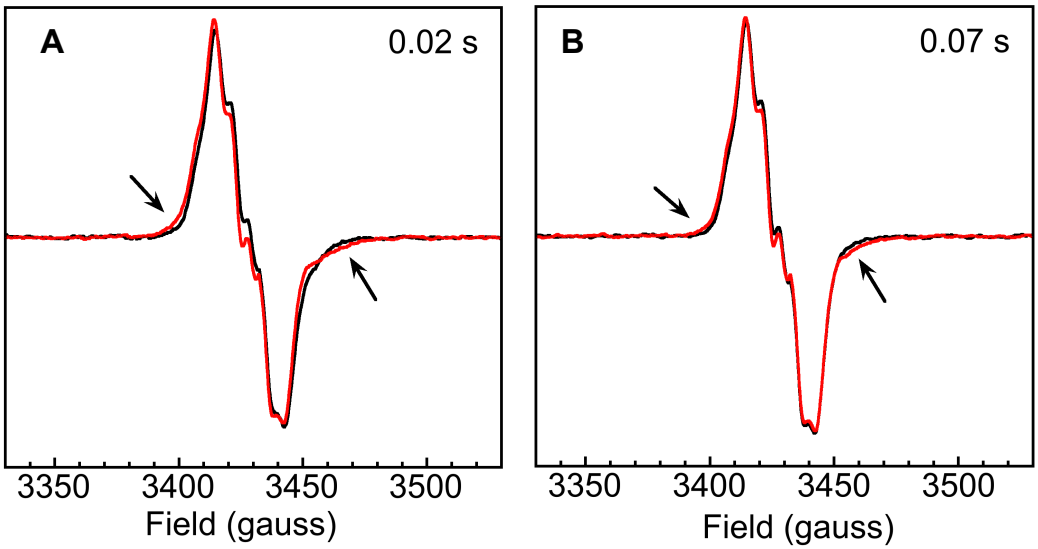

Figure S15. Hyperfine broadening by ^{57}Fe (I = 1/2) in the X-band EPR spectra of freeze-quenched samples from the reaction of wt UndA implies accumulation of the Fe_2(III/IV)_ complex. Samples were prepared by mixing (at 5 °C) a solution of 1.2 mM UndA, 2.2 mM (1.8 equiv) Fe(II), and 3.6 mM LA with an equal volume of O_2-saturated buffer (~1.8 mM O_2) and freeze-quenching after a reaction time of (***A***) 0.02 s or (***B***) 0.07 s. The spectra of samples prepared with ^{57}Fe are shown in red, and the spectra of samples prepared with natural-abundance Fe (~97.8% isotopes ^{54}Fe, ^{56}Fe, and ^{58}Fe, all having I = 0,) are shown in black. The arrows indicate the subtle ^{57}Fe hyperfine broadening arising from the ^{57}Fe hyperfine coupling in the Fe_2(III/IV) complex. Spectrometer conditions were: temperature = 20 K, modulation amplitude = 4 G, microwave frequency = 9.625 GHz, microwave power = 20 μW.

Table S1. Primers used for the generation of UndA variants.

Variant		Sequence
Y71F	Forward	5′-GAACAGTTCGCCCTGTTCATGGCGCAAAACCTG-3′
	Reverse	5′-CAGGTTTTGCGCCATGAACAGGGCGAACTGTTC-3′
Y107F	Forward	5′-CGAGCTCAATCATGCCGATTTCTGGGTGCACT-3′
	Reverse	5′-AGTGCACCCAGAAATCGGCATGATTGAGCTCG-3′
Y197F	Forward	5′-CTGAAGATGCATGCCCAGTTCGACGACGCC-3′
	Reverse	5′-GGCGTCGTCGAACTGGGCATGCATCTTCAG-3′
W190F	Forward	5′-TTTCTGAAGATGCATGCCCAGTA-3′
	Reverse	5′-CTTCATGGCACGTTTGCGAT -3′
E159A	Forward	5′-CCAACTACGCCATTGCAGGGGCCACGGGCGA-3′
	Reverse	5′-TCGCCCGTGGCCCCTGCAATGGCGTAGTTGG-3′
H201A	Forward	5′-CAGTACGACGACGCCGCGCCCTGGGAAGCGCTG-3′
	Reverse	5′-CAGCGCTTCCCAGGGCGCGGCGTCGTCGTACTG-3′
D198A	Forward	5′-TGCATGCCCAGTACGCCGACGCCCATCCCTG-3′
	Reverse	5′-CAGGGATGGGCGTCGGCGTACTGGGCATGCA-3′

Table S2. Data collection and refinement statistics for the x-ray structures of UndA[⊥].

	Fe(II)-soaked LA-bound UndA (native)	**Fe(II)-soaked LA-bound UndA (Fe anomalous)**
Data collection		
Wavelength	0.97857 Å	1.72200 Å
Space group	$P222_1$	$P222_1$
Cell dimensions		
a, b, c (Å)	68.009, 74.148, 142.563	67.962, 74.020, 142.455
α, β, γ (°)	90, 90, 90	90, 90, 90
Resolution (Å)	50-1.86 (1.89-1.86)*	80-2.61 (2.66-2.61)*
R_{merge}	0.058 (0.469)	0.076 (0.163)
$< I/\sigma >$	29.1 (3.0)	22.5 (12.1)
$CC_{1/2}$	0.942	0.977
Completeness (%)	98.9 (100.0)	100.0 (99.9)
Redundancy	5.8 (6.1)	6.3 (5.3)
Refinement		
Resolution (Å)	1.86	
No. reflections	60130	
R_{work}/R_{free}	0.1978/0.2166	
No. atoms	4307	
Protein	4019	
Ligand/ion	38	
Water	250	
B-factors		
Protein	25.3	
Ion/Ligand	28.4	
Water	25.7	
r.m.s deviations		
Bond lengths (Å)	0.003	
Bond angles (°)	0.530	
PDB accession code	6P5Q	

[⊥]A single crystal was used to collect both datasets.

*Highest resolution shell is shown in parenthesis.

Table S3. Parameters used for fitting the EXAFS data shown in Figure S4.

	Scatterer	Coordination number	Distance (Å)	σ^2
aerobically isolated	Fe	0.75	3.21	0.00207
	C/N/O	1	1.86	0.01250
	C/N/O	4	2.1	0.00797
	C/N/O	1	2.57	0.00229
sodium dithionite reduced	Fe	0.75	3.97	0.00903
	C/N/O	2	2.22	0.00430
	C/N/O	2.5	2.31	0.00446
	C/N/O	2	3.17	0.00936
	C/N/O	3	3.66	0.00645

Table S4. Parameters used for fitting the EXAFS data shown in Figure S5.

	Scatterer	Coordination number	Distance (Å)	σ^2
No Fe-Fe vector	C/N/O	3	2.15	0.00462
	C/N/O	2	2.32	0.00320
	C/N/O	3	2.91	0.00910
	C/N/O	5	3.22	0.00375
Two Fe-Fe vectors	Fe	0.3	2.94	0.00062
	Fe	0.6	3.25	0.00394
	C/N/O	2	2.13	0.00149
	C/N/O	1.5	2.26	0.00250

References

1. Rui, Z.; Li, X.; Zhu, X.; Liu, J.; Domigan, B.; Barr, I.; Cate, J. H.; Zhang, W., Microbial biosynthesis of medium-chain 1-alkenes by a nonheme iron oxidase. *Proc. Natl. Acad. Sci. U. S. A.* **2014,** *111* (51), 18237-18242.

2. Stookey, L., Ferrozine - a new spectrophotometric reagent for iron. *Anal. Chem.* **1970,** *42* (7), 779-&.

3. George, G. N., EXAFSPAK. SSRL, SLAC, Stanford University: Stanford, CA.

4. Tenderholt, A.; Hedman, B.; Hodgson, K. O., PySpline: A modern, cross-platform program for the processing of raw averaged XAS edge and EXAFS data. *X-Ray Absorption Fine Structure-Xafs13* **2007,** *882*, 105-+.

5. Rehr, J. J.; Kas, J. J.; Vila, F. D.; Prange, M. P.; Jorissen, K., Parameter-free calculations of X-ray spectra with FEFF9. *Phys. Chem. Chem. Phys.* **2010,** *12* (21), 5503-5513.

6. Otwinowski, Z.; Minor, W., Processing of X-ray diffraction data collected in oscillation mode. *Method. Enzymol.* **1997,** *276*, 307-326.

7. McCoy, A. J.; Grosse-Kunstleve, R. W.; Adams, P. D.; Winn, M. D.; Storoni, L. C.; Read, R. J., Phaser crystallographic software. *J. Appl. Crystallogr.* **2007,** *40*, 658-674.

8. Winn, M. D.; Ballard, C. C.; Cowtan, K. D.; Dodson, E. J.; Emsley, P.; Evans, P. R.; Keegan, R. M.; Krissinel, E. B.; Leslie, A. G.; McCoy, A.; McNicholas, S. J.; Murshudov, G. N.; Pannu, N. S.; Potterton, E. A.; Powell, H. R.; Read, R. J.; Vagin, A.; Wilson, K. S., Overview of the CCP4 suite and current developments. *Acta Crystallogr. D* **2011,** *67* (Pt 4), 235-242.

9. Murshudov, G. N.; Skubak, P.; Lebedev, A. A.; Pannu, N. S.; Steiner, R. A.; Nicholls, R. A.; Winn, M. D.; Long, F.; Vagin, A. A., REFMAC5 for the refinement of macromolecular crystal structures. *Acta Crystallogr. D* **2011,** *67*, 355-367.

10. Emsley, P.; Lohkamp, B.; Scott, W. G.; Cowtan, K., Features and development of Coot. *Acta Crystallogr. D* **2010,** *66*, 486-501.

11. Adams, P. D.; Afonine, P. V.; Bunkóczi, G.; Chen, V. B.; Davis, I. W.; Echols, N.; Headd, J. J.; Hung, L.-W.; Kapral, G. J.; Grosse-Kunstleve, R. W.; McCoy, A. J.; Moriarty, N. W.; Oeffner, R.; Read, R. J.; Richardson, D. C.; Richardson, J. S.; Terwilliger, T. C.; Zwart, P. H., PHENIX: a comprehensive Python-based system for macromolecular structure solution. *Acta Crystalogr. D, Biol. crystallogr.* **2010,** *66* (Pt 2), 213-221.

12. Chen, V. B.; Arendall, W. B.; Headd, J. J.; Keedy, D. A.; Immormino, R. M.; Kapral, G. J.; Murray, L. W.; Richardson, J. S.; Richardson, D. C., MolProbity: all-atom structure validation for macromolecular crystallography. *Acta. Crystallogr. D Biol. Crystallogr.* **2010,** *66*, 12-21.

13. Bollinger, J.; Edmondson, D.; Huynh, B.; Filley, J.; Norton, J.; Stubbe, J., Mechanism of Assembly of The Tyrosyl Radical Dinuclear Iron Cluster Cofactor of Ribonucleotide Reductase. *Science* **1991,** *253* (5017), 292-298.

14. Price, J. C.; Barr, E. W.; Tirupati, B.; Bollinger, J. M., Jr.; Krebs, C., The first direct characterization of a high-valent iron intermediate in the reaction of an alpha-ketoglutarate-dependent dioxygenase: A high-spin Fe(IV) complex in taurine/alpha-ketoglutarate dioxygenase (TauD) from *Escherichia coli*. *Biochemistry* **2003,** *42* (24), 7497-7508.

15. Ravi, N.; Bollinger, J. M., Jr.; Huynh, B. H.; Edmondson, D. E.; Stubbe, J., Mechanism of Assembly of the Tyrosyl Radical-Diiron(Iii) Cofactor of *Escherichia-Coli* Ribonucleotide Reductase 1. Mössbauer Characterization of the Diferric Radical Precursor. *J. Am. Chem. Soc.* **1994,** *116* (18), 8007-8014.

16. Jiang, W.; Hoffart, L. M.; Krebs, C.; Bollinger, J. M., Jr., A manganese(IV)/iron(IV) intermediate in assembly of the manganese(IV)/iron(III) cofactor of *Chlamydia trachomatis* ribonucleotide reductase. *Biochemistry* **2007,** *46* (30), 8709-8716.

17. Manley, O. M.; Fan, R.; Guo, Y.; Makris, T. M., Oxidative Decarboxylase UndA Utilizes a Dinuclear Iron Cofactor. *J. Am. Chem. Soc.* **2019,** *141* (22), 8684-8688.

18. Kauffmann, K. E.; Popescu, C. V.; Dong, Y. H.; Lipscomb, J. D.; Que, L.; Münck, E., Mössbauer evidence for antisymmetric exchange in a diferric synthetic complex and diferric methane monooxygenase. *J. Am. Chem. So.c* **1998,** *120* (34), 8739-8746.

19. Shu, L.; Broadwater, J.; Achim, C.; Fox, B.; Munck, E.; Que, L., EXAFS and Mössbauer characterization of the Diiron(III) site in stearoyl-acyl carrier protein Delta(9-) desaturase. *J. Biol. Inorg. Chem.* **1998,** *3* (4), 392-400.

20. True, A.; Scarrow, R.; Randall, C.; Holz, R.; Que, L., Jr., EXAFS studies of uteroferrin and its anion complexes. *J. Am. Chem. Soc.* **1993,** *115* (10), 4246-4255.

21. Dewitt, J.; Bentsen, J.; Rosenzweig, A.; Hedman, B.; Green, J.; Pilkington, S.; Papaefthymious, G.; Dalton, H.; Hodgson, K.; Lippard, S., X-ray Absorption, Mössbauer, and EPR studies of the dinuclear iron center in the hydroxylase component of methane monooxygenase. *J. Am. Chem. Soc.* **1991,** *113* (24), 9219-9235.

22. Scarrow, R.; Maroney, M.; Palmer, S.; Que, L., Jr.; Roe, A.; Salower, S.; Stubbe, J., EXAFS studies of binuclear iron proteins - hemerythrin and ribonucleotide reductase. *J. Am. Chem. Soc.* **1987,** *109* (25), 7857-7864.

23. Jasniewski, A.; Knoot, C.; Lipscomb, J.; Que, L., A Carboxylate Shift Regulates Dioxygen Activation by the Diiron Nonheme beta-Hydroxylase CmIA upon Binding of a Substrate-Loaded Nonribosomal Peptide Synthetase. *Biochemistry* **2016,** *55* (41), 5818-5831.

24. Rudd, D.; Sazinsky, M.; Lippard, S.; Hedman, B.; Hodgson, K., X-ray, absorption spectroscopic study of the reduced hydroxylases of methane monooxygenase and toluene/o-xylene monooxygenase: Differences in active site structure and effects of the coupling proteins MMOB and ToMOD. *Inorg. Chem.* **2005,** *44* (13), 4546-4554.

25. Makris, T.; Chakrabarti, M.; Munck, E.; Lipscomb, J., A family of diiron monooxygenases catalyzing amino acid beta-hydroxylation in antibiotic biosynthesis. *Proc. Natl. Acad. Sci. U.S.A.* **2010,** *107* (35), 15391-15396.

26. Fox, B.; Hendrich, M.; Surerus, K.; Andersson, K.; Froland, W.; Lipscomb, J.; Münck, E., Mossbauer, Epr, And Endor Studies Of The Hydroxylase And Reductase Components Of Methane Monooxygenase From Methylosinus-Trichosporium Ob3b. *J. Am. Chem. Soc.* **1993,** *115* (9), 3688-3701.

27. Davydov, R.; Kuprin, S.; Gräslund, A.; Ehrenberg, A., Electron paramagnetic resonance study of the mixed-valent diiron center in *Escherichia coli* ribonucleotide reductase produced by reduction of radical-free protein-R2 at 77 K. *J. Am. Chem. Soc.* **1994,** *116* (24), 11120-11128.

28. Schwarzenbacher, R.; Stenner-Liewen, F.; Liewen, H.; Robinson, H.; Yuan, H.; Bossy-Wetzel, E.; Reed, J. C.; Liddington, R. C., Structure of the *Chlamydia* protein CADD reveals a redox enzyme that modulates host cell apoptosis. *J Biol Chem* **2004,** *279* (28), 29320-29324.

29. Ng, T. L.; Rohac, R.; Mitchell, A. J.; Boal, A. K.; Balskus, E. P., An N-nitrosating metalloenzyme constructs the pharmacophore of streptozotocin. *Nature* **2019,** *566* (7742), 94-99.

30. Sturgeon, B. E.; Burdi, D.; Chen, S.; Huynh, B. H.; Edmondson, D. E.; Stubbe, J.; Hoffman, B. M., Reconsideration of X, the diiron intermediate formed during cofactor assembly in *E. coli* Ribonucleotide Reductase. *J. Am. Chem. Soc.* **1996,** *118* (32), 7551-7557.